Trajectory Tracking Control of Omnidirectional Mobile Robots: a Model-Free Control-based Apprroach

Pham Anh Tuan[1] and Nguyen Manh Linh[2,*]

[1] *Hanoi University of Science and Technology. E-mail:tuan.pa192147@sis.hust.edu.vn*

[2,*] *Hanoi University of Science and Technology. E-mail: linh.nguyenmanh@hust.edu.vn*

Controlling the motion of mobile robots, especially those equipped with Mecanum wheels is challenging due to the existence of disturbances and model uncertainties. In this paper, instead of trying to build a precise model for control design, the model-free control which replaces all the unknown complex mathematical parts with an ultra-local model is chosen. Then, an iPDSMC controller that combines the classical iPD and a double power rate sliding mode controller is proposed to improve the control system performance. The proposed strategy guarantees that even with a low bandwidth extended state observer used to continuously update the unknown parts of the plant, the tracking performance is maintained. The effectiveness of the proposed strategy is verified by both theoretical analysis and numerical simulations

Keywords: Omnidirectional mobile robot; Model-free control; Ultra-local model; Extended-state observer; Sliding mode control

1. INTRODUCTION

Mobile robots, particularly the omnidirectional ones that are equipped with Mecanum wheels, have gained widespread adoption in various industries due to their exceptional capabilities. These robots offer significant advantages, making them highly desirable for numerous applications. The Mecanum wheel-based mobile robots possess true omnidirectional capabilities, allowing them to move in multiple directions with ease. This exceptional maneuverability enables them to navigate through narrow spaces and crowded environments, where conventional wheeled robots would struggle. By effortlessly moving forward, backward, sideways,

Table 1. List of Abbreviations

Abbreviation	Full Form
4-MWMR	Four Mecanum Wheeled Mobile Robot
MPC	Model Predictive Control
MFC	Model Free Control
SMC	Sliding Mode Control
iPD	Intelligent Proportional-Derivative
iPDSMC	Intelligent Proportional-Derivative Sliding Mode Control
ULM	Ultra-local Model
ULMFC	Ultra-local Model-free Control
ESO	Extended state observe
LESO	Linear Extended state observe

and even rotating in tight areas, these robots excel in optimizing productivity and efficiency. These exceptional capabilities have led to the widespread adoption of mobile robots equipped with Mecanum wheels in various industries, where their applications have been notably pronounced. These robots have proven to be immensely valuable in warehouse automation [1], hospital logistics [2], services [3], industrial field [4],...

With such practical applications as mentioned above, trajectory tracking has become a fundamental and essential problem in mobile robot motion control, drawing significant attention in the field of mobile robot research. Accurate trajectory tracking is of utmost importance for 4-MWMR, as it directly reflects the effectiveness and performance of the tracking process.

In literature, control strategies can be roughly categorized into two main types: model-based and model-free approaches. Model-based control methods rely on mathematical models that describe the dynamics or kinematics of the system being controlled. Based on the kinematic model, several research papers have proposed control strategies for Mecanum mobile robots such as PID controller in [5–7] or LQR in [8]. It is worth mentioning that while the kinematic model-based control strategies provide simplified representations of the robot's motion, they disregard the effects of inertia and motor torque limitations, assuming that the desired velocities will be precisely and instantaneously achieved. However, in the case of heavier robots or those with less powerful actuators, relying solely on a kinematic controller may not be adequate. These robots may require additional time to accelerate or may be limited by their actuator capabilities. Due to the limitations of the kinematic model, many researchers have developed controllers based on the dynamic model. Prominent examples of control strategies based on the dynamic model include: MPC controller [9–12], backstepping control [13–15], and sliding mode control. While the MPC controller can provide robustness against the model uncertainties and disturbances, it requires an accurate mathematical model of the plant. And it is important to note that SMC can introduce chattering phenomena, characterized by high-frequency oscillations around the sliding surface. This chattering effect can result in increased wear and tear on the actuators and potentially affect the overall system stability and performance. Numerous studies have been conducted to reduce and eliminate chattering associated with controlling the 4-MWMR such as super-twisting sliding mode control [16], adaptive second-order sliding mode [17], nonsingular terminal sliding mode [18], etc. However, the success of these control methods is strongly governed by the accuracy of the 4-MWMR's mathematical model. Neural networks-based control strategies are also remarkable since the reliance on explicit model assumptions can be minimized [19]. However, this approach requires a significant amount of data.

To address the challenges of model-based control, a model-free control technique has been developed, with one prominent method that has garnered significant attention ultra-local model-free control [20, 21]. It works with an ultra-local model continuously updated via input-output information. The greatest advantage of the ULMFC is that it does not rely on mathematical models or even ultra-local models during the tuning process of the controller. Due to the need for continuous updating of the ultra-local model (ULM), various research studies have employed different methods to address this challenge. Some notable approaches include: approximated by a piecewise function [21], sliding mode observer [**bib22**], extended state observer [22], dual disturbance observers [23], etc. In this paper, we utilize the linear extended state observer (LESO) [24, 25], a simple yet highly effective observer that can simultaneously estimate unmodeled dynamics and external disturbances. Moreover, in cases where estimation errors may occur in the observer, the sliding mode control is employed to mitigate these discrepancies. In the previous section, we mentioned several improved methods for the SMC. Although significant improvements have been made in terms of performance enhancement and reducing chattering phenomena, some of these algorithms are too complex to be practically implemented. In this research, to strike a balance between real-world applicability, performance enhancement, and reduction of chattering phenomenon, the SMC with improved reaching law is adopted and clarified in the subsequent sections.

The remainder of this paper is organized as follows. In section II, we construct a dynamic model of the 4-MWMR. Next, the process of designing the controller and observer will be presented in section III. The stability of the controller and observer is carried out in section IV. Finally, the simulation scenarios and conclusions are conducted in sections V and VI, respectively.

Table 2. NOMENCLATURE

Symbol	Description
$\boldsymbol{q}_q = \begin{bmatrix} x_q & y_q & \phi \end{bmatrix}^T$	Robot position in inertial frame
$\boldsymbol{q} = \begin{bmatrix} x_r & y_r & \phi \end{bmatrix}^T$	Robot position in body frame
$\boldsymbol{q}_{ref}$	The reference trajectory
θ_i	Angular velocity of the ith wheel
$\boldsymbol{\tau}_c = \begin{bmatrix} \tau_1 & \tau_2 & \tau_3 & \tau_4 \end{bmatrix}^T$	External generalized force generated by four motors
$\boldsymbol{f} = \begin{bmatrix} f_1 & f_2 & f_3 & f_4 \end{bmatrix}^T$	Static friction of 4 wheels
D_θ	Wheel's viscous friction coefficient
I_w	The moment of inertia of the wheel around its center of revolution
I_z	Robot's moment of inertial around the rotation center
m	Total mass of the FMWMR
R	The radius of Mecanum wheel
a	Half width of the FMWNR
b	Half length of the FMWMR
$\boldsymbol{R}(\phi)$	Coordinate Transformation Matrix between Inertial and Body frame

2. System Description

The mathematical model described here is intended exclusively for simulation purposes and is not intended for use in controller design.

2.1. Kinematic of FMWMR

To obtain the kinematic model of the 4-MWMR, we assume that

- The robot moves on a flat horizontal plane
- The 4-MWMR is composed of a rigid body

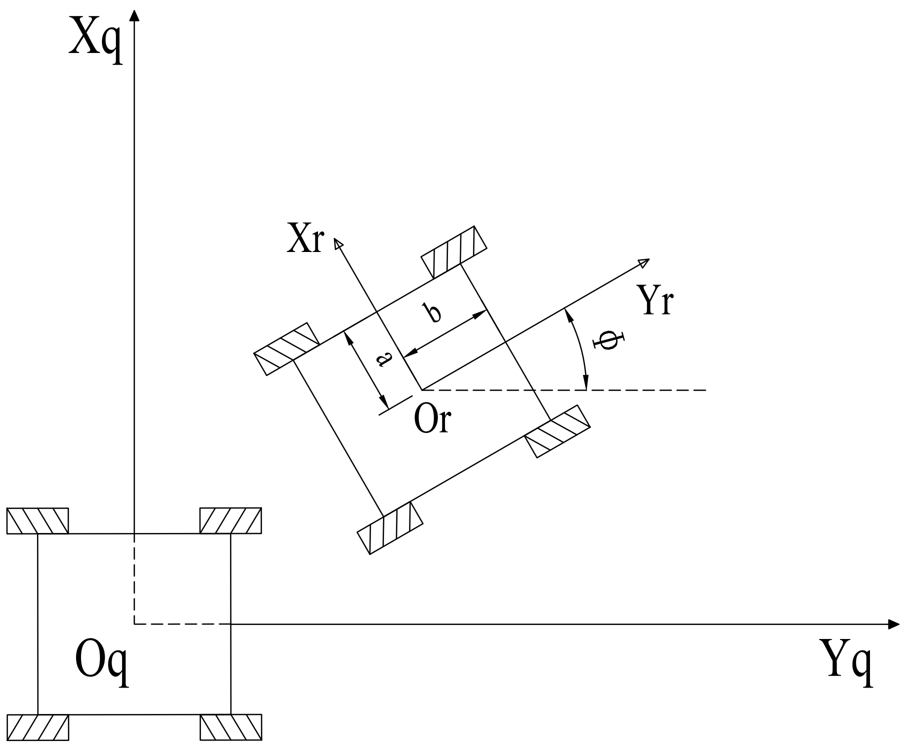

Fig. 1. Coordinate system assignment of the 4-MWMR

- There is no slipping and skidding when the robot moves

Based on extensive and meticulous research conducted over the years, the kinematic model of the 4-MWMR with coordinate system assignment shown in Fig. 1 can be described by

$$\begin{bmatrix} \dot{\theta}_1 \\ \dot{\theta}_2 \\ \dot{\theta}_3 \\ \dot{\theta}_4 \end{bmatrix} = \frac{1}{R} \begin{bmatrix} 1 & 1 & (a+b) \\ -1 & 1 & -(a+b) \\ 1 & 1 & -(a+b) \\ -1 & 1 & (a+b) \end{bmatrix} \begin{bmatrix} \dot{x}_r \\ \dot{y}_r \\ \dot{\phi} \end{bmatrix} \tag{1}$$

Define a Jacobian matrix as

$$\boldsymbol{J} = \begin{bmatrix} 1 & 1 & (a+b) \\ -1 & 1 & -(a+b) \\ 1 & 1 & -(a+b) \\ -1 & 1 & (a+b) \end{bmatrix} \tag{2}$$

Since $\boldsymbol{J}$ is a non-square matrix, there exists a pseudo-inverse of $\boldsymbol{J}$ such that

$$\boldsymbol{J}^{+} = \frac{1}{4} \begin{bmatrix} 1 & -1 & 1 & -1 \\ 1 & 1 & 1 & 1 \\ \frac{1}{a+b} & \frac{-1}{a+b} & \frac{-1}{a+b} & \frac{1}{a+b} \end{bmatrix} \tag{3}$$

Substituting (2) into (1), it yields

$$\begin{bmatrix} \dot{x}_r \\ \dot{y}_r \\ \dot{\phi} \end{bmatrix} = R\boldsymbol{J}^{+} \begin{bmatrix} \dot{\theta}_1 \\ \dot{\theta}_2 \\ \dot{\theta}_3 \\ \dot{\theta}_4 \end{bmatrix} \tag{4}$$

The constraint between the inertial and body frames can be described by

$$\begin{bmatrix} \dot{x}_q \\ \dot{y}_q \\ \dot{\phi} \end{bmatrix} = \boldsymbol{R}(\phi) \begin{bmatrix} \dot{x}_r \\ \dot{y}_r \\ \dot{\phi} \end{bmatrix} \tag{5}$$

$$\boldsymbol{R}(\phi) = \begin{bmatrix} cos(\phi) & -sin(\phi) & 0 \\ sin(\phi) & cos(\phi) & 0 \\ 0 & 0 & 1 \end{bmatrix}. \tag{6}$$

2.2. Dynamic model of FMWMR

As proposed in [26] and mentioned in [16], the dynamic model of the 4-MWMR can be expressed based on the Lagrange's equation as follows:

$$\begin{aligned}
&2(\boldsymbol{\tau_c} - \boldsymbol{F_0}) - \frac{\partial D_\theta \sum_{i=1}^{4} \dot{\theta}_i^2}{\partial \theta} \\
&= \frac{\partial}{\partial t} \frac{\partial \left(m \left(\dot{x}_q^2 + \dot{y}_q^2 \right) + J_z \dot{\phi}^2 + J_\omega \sum_{i=} \dot{\theta}_i{}^2 \right)}{\partial \theta} \\
&- \frac{\partial \left(m \left(x_q{}^2 + \dot{y}_q^2 \right) + J_z \dot{\phi}^2 + J_\omega \sum_{i=1}^{4} \dot{\theta}_i^2 \right)}{\partial \theta},
\end{aligned} \tag{7}$$

In which,

$$\boldsymbol{\tau_c} = \boldsymbol{M}\ddot{\boldsymbol{\theta}} + D_\theta \dot{\boldsymbol{\theta}} + \boldsymbol{F_0} \tag{8}$$

$$\boldsymbol{F_0} = \boldsymbol{f} \cdot \begin{bmatrix} sign(\theta_1) & sign(\theta_2) & sign(\theta_3) & sign(\theta_4) \end{bmatrix} \tag{9}$$

$$\mathbf{M} = \begin{bmatrix} C & -B & B & D \\ -B & C & D & B \\ B & D & C & -B \\ D & B & -B & C \end{bmatrix} \tag{10}$$

With

$$\begin{aligned}
A &= \frac{m \cdot R^2}{8}, \\
B &= \frac{I_z \cdot R^2}{16 \cdot (W + L)^2}, \\
C &= A + B + I_W, \\
D &= A - B
\end{aligned}$$

Considering the unknown dynamic disturbances and uncertainties which always exist in practice, then (8) can be rewritten as:

$$\boldsymbol{\tau_c} + \boldsymbol{\tau_d} = (\boldsymbol{M} + \Delta \boldsymbol{M})\ddot{\boldsymbol{\theta}} + (D_\theta + \Delta D_\theta)\, \dot{\boldsymbol{\theta}} + \boldsymbol{F_0} + \Delta \boldsymbol{F_0} \tag{11}$$

In which, $\boldsymbol{\tau_d}$, $\Delta\boldsymbol{M}$, ΔD_θ and $\Delta\boldsymbol{F_0}$ represent the unknown disturbances. Hence,

$$\boldsymbol{\tau_c} + \boldsymbol{\tau_d} + \boldsymbol{H_d} = \boldsymbol{M}\ddot{\boldsymbol{\theta}} + D_\theta\dot{\boldsymbol{\theta}} + \boldsymbol{F_0} \tag{12}$$

with $\boldsymbol{H}_d = -\Delta M\ddot{\theta} - \Delta D_\theta\dot{\theta} - \Delta F_0$.

$\boldsymbol{\tau}_d + \boldsymbol{H}_d$ is defined as the lumped disturbance in our system. Now, substitute (4) and (5) into (12), the dynamic model of the 4-MWMR can be obtained after a fundamental manipulation and described by:

$$\begin{aligned}\ddot{\boldsymbol{q}} = &-\left(\zeta^+(\phi)\dot{\zeta}(\phi) + D_\theta\zeta^+(\phi)M^{-1}\zeta(\phi)\right)\dot{\boldsymbol{q}} \\ &+ R\zeta^+(\phi)M^{-1}\left(\boldsymbol{\tau_c} + \boldsymbol{\tau_d} + \boldsymbol{H_d} - \boldsymbol{F_0}\right)\end{aligned} \tag{13}$$

where,

$$\boldsymbol{q} = \begin{bmatrix} x_q & y_q & \Phi \end{bmatrix}^T \tag{14}$$

$$\zeta^+(\phi) = \frac{1}{4}\begin{bmatrix} \sqrt{2}\cos(\phi_a) & -\sqrt{2}\sin(\phi_a) & \sqrt{2}\cos(\phi_a) & -\sqrt{2}\sin(\phi_a) \\ \sqrt{2}\sin(\phi_a) & \sqrt{2}\cos(\phi_a) & \sqrt{2}\sin(\phi_a) & \sqrt{2}\cos(\phi_a) \\ \frac{1}{a+b} & -\frac{1}{a+b} & -\frac{1}{a+b} & \frac{1}{a+b} \end{bmatrix} \tag{15}$$

$$\zeta = \begin{bmatrix} \sqrt{2}\cos(\phi_a) & \sqrt{2}\sin(\phi_a) & a+b \\ -\sqrt{2}\sin(\phi_a) & \sqrt{2}\cos(\phi_a) & -(a+b) \\ \sqrt{2}\cos(\phi_a) & \sqrt{2}\sin(\phi_a) & -(a+b) \\ -\sqrt{2}\sin(\phi_a) & \sqrt{2}\cos(\phi_a) & a+b \end{bmatrix} \tag{16}$$

$$\dot{\zeta} = \dot{\phi}\begin{bmatrix} -\sqrt{2}\sin(\phi_a) & \sqrt{2}\cos(\phi_a) & 0 \\ -\sqrt{2}\cos(\phi_a) & -\sqrt{2}\sin(\phi_a) & 0 \\ -\sqrt{2}\sin(\phi_a) & \sqrt{2}\cos(\phi_a) & 0 \\ -\sqrt{2}\cos(\phi_a) & -\sqrt{2}\sin(\phi_a) & 0 \end{bmatrix} \tag{17}$$

Since the model-free controller is employed in this research, the control design is not based on the dynamic model (13). However, the performance of the controller that going to be designed must be verified by using (13).

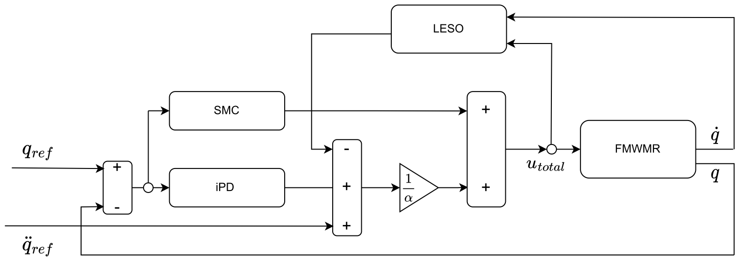

Fig. 2. Control scheme of the proposed MFC

3. Control Design

In this section, the MFC design is presented. The block diagram of the proposed MFC is shown in Fig. 2, which consists of a LESO that can simultaneously estimate unmodeled dynamics and external disturbances, an iPD controller to track the reference trajectory, and an SMC to mitigate the remaining estimation errors. The control design of the proposed control system is carried out in the next subsections.

3.1. Ultra-local model-free control: general principles

The main concept of the ultra-local model-free is using a local model that is continuously updated via a control signal and the system's output. Consider the following dynamic equation:

$$y^{(v)} = F + \alpha.u \tag{18}$$

in which,

- v is the derivative order of y, which needs to be selected appropriately for the plant. In our implementation $v = 2$
- α is a constant which must be tuned appropriately
- F encompasses the plant's unmodeled dynamics, uncertainty, and external disturbances

- u is the control signal

Since the goal of our research is trajectory tracking control, (18) is rewritten as:

$$\ddot{\boldsymbol{q}} = \boldsymbol{F} + \alpha \boldsymbol{u} \tag{19}$$

Define $\mathbf{e}$ as the tracking error, which means

$$\mathbf{e} = \mathbf{q}_{ref} - \mathbf{q} \tag{20}$$

Based on the ultra-local model [20], an *iPD* controller is employed as following:

$$\boldsymbol{u} = \frac{1}{\alpha}(K_p \boldsymbol{e} + K_D \dot{\boldsymbol{e}} + \ddot{\boldsymbol{q}}_{\boldsymbol{ref}} - \hat{\boldsymbol{F}}) \tag{21}$$

where K_p and K_D are positive gains.

By substituting (21) into (19), it can easily be deduced that

$$\ddot{\boldsymbol{e}} + K_p \boldsymbol{e} + K_D \dot{\boldsymbol{e}} = \hat{\boldsymbol{F}} - \boldsymbol{F} \tag{22}$$

or

$$\ddot{\boldsymbol{e}} + K_p \boldsymbol{e} + K_D \dot{\boldsymbol{e}} = \tilde{\boldsymbol{F}} \tag{23}$$

In which,

- $\hat{\boldsymbol{F}}$ is the estimation of $\boldsymbol{F}$ using an extended state observer that is going to be discussed in the next subsection.

- $\tilde{\boldsymbol{F}} = \hat{\boldsymbol{F}} - \boldsymbol{F}$ is the estimation error

It can be realized from (23) that if the observer is perfect, i.e., $\tilde{\boldsymbol{F}} \approx 0$, then the dynamic of the tracking error can be described by

$$\ddot{\boldsymbol{e}} + K_p.\boldsymbol{e} + K_D.\dot{\boldsymbol{e}} = 0 \tag{24}$$

Meaning that the tracking performance is now only dependent on K_p and K_D of the *iPD* controller.

3.2. Linear Extended State Observer Design

As has been discussed, the disturbance observer plays an essential role in affecting the quality of the control system. Hence, this subsection focuses on the observer design. The Extended state observer (ESO) was initially introduced by Han [24] as a component of the ARDC, which is capable of simultaneously estimating unmodeled dynamics, parameter uncertainties, and external disturbances by treating them as a lumped perturbation. The robustness and outstanding performance of the non-linear extended state observer have attracted significant attention from researchers and have been validated through practical applications. However, one disadvantage of this observer is that the tuning of multiple parameters is complicated. To address this issue, Gao [25] proposes to use linear feedback rather than non-linear feedback, resulting in the development of the LESO in which only one parameter, i.e., the observer's bandwidth ω_0, needs to be adjusted. In our research, the LESO is adopted to estimate the lumped disturbance F. In detail, define the state variables as:

$$\begin{cases} \boldsymbol{x_1} = \dot{\boldsymbol{q}} \\ \boldsymbol{x_2} = \boldsymbol{F} \end{cases} \tag{25}$$

Define $\boldsymbol{f}$ and $\dot{\boldsymbol{f}}$ are the first and the second order differentiation of the unknown lumped disturbance $\boldsymbol{F}$, i.e., $\boldsymbol{f} = \dot{\boldsymbol{F}}$ and $\dot{\boldsymbol{f}} = \ddot{\boldsymbol{F}}$

Assumption 1: There exists positive number ε_1 and ε_2 such that $\boldsymbol{f}$ and its differentiation $\dot{\boldsymbol{f}}$ are bounded by

$$||\boldsymbol{f}|| \leq \varepsilon_1 \tag{26}$$

$$||\dot{\boldsymbol{f}}|| \leq \varepsilon_2 \tag{27}$$

Base on (25), (19) can be rewritten in state-space form as:

$$\begin{cases} \dot{x}_1 = \boldsymbol{x_2} + \alpha \boldsymbol{u} \\ \dot{x}_2 = \boldsymbol{f} \end{cases} \tag{28}$$

Since we can directly measure $\boldsymbol{x}_1 = \dot{\boldsymbol{q}}$ by an encoder in practice, the LESO can be designed as:

$$\begin{cases} \dot{\hat{\boldsymbol{x}}}_{\boldsymbol{1}} = \hat{\boldsymbol{x}}_{\boldsymbol{2}} + \alpha.\boldsymbol{u} + \beta_1.(\boldsymbol{x}_1 - \hat{\boldsymbol{x}}_1) \\ \dot{\hat{\boldsymbol{x}}}_{\boldsymbol{2}} = \beta_2(\boldsymbol{x}_1 - \hat{\boldsymbol{x}}_1) \end{cases} \tag{29}$$

In (29), $\hat{\boldsymbol{x}}_{\boldsymbol{1}} = \dot{\hat{\boldsymbol{q}}}$ and $\hat{x}_2 = \hat{\boldsymbol{F}}$ are the estimation of $\dot{\boldsymbol{q}}$ and $\boldsymbol{F}$, respectively. The two remaining parameters β_1 and β_2 are the observer's gains that must be tuned appropriately. Now, subtract (29) from (28), the estimation error can be formulated by:

$$\begin{cases} \dot{\tilde{x}}_1 = \tilde{x}_2 - \beta_1 \tilde{x}_1 \\ \dot{\tilde{x}}_2 = \boldsymbol{f} - \beta_2 \tilde{x}_1 \end{cases} \tag{30}$$

Differentiate both sides of (30), a fundamental manipulation yields:

$$\begin{cases} \ddot{\tilde{x}}_1 + \beta_1 \dot{\tilde{x}}_1 + \beta_2 \tilde{x}_1 & = \boldsymbol{f} \\ \ddot{\tilde{x}}_2 + \beta_1 \dot{\tilde{x}}_2 + \beta_2 \tilde{x}_2 & = \beta_1 \boldsymbol{f} + \dot{\boldsymbol{f}} \end{cases} \tag{31}$$

Since $\tilde{x}_1$, $\tilde{x}_2$ and $\boldsymbol{f}$ are the same size, i.e., $[3 \times 1]$, a simple Laplace transformation on both sides of (31) gives

$$\begin{aligned} \frac{\tilde{x}_{1,i}}{f_i} &= \frac{1}{p^2 + \beta_1 p + \beta_2} \\ \frac{\tilde{x}_{2,i}}{\beta_1 f_i + \dot{f}_i} &= \frac{1}{p^2 + \beta_1 p + \beta_2} \end{aligned} \tag{32}$$

In which, $i = [1, 2, 3]$ and p is the Laplace operator. Now, based on (32) and taking assumption (27) into account, the following two conclusions can be drawn.

First, the stability and the dynamic of the *LESO* can be guaranteed by tuning the parameters of the following characteristic equation

$$p^2 + \beta_1 p + \beta_2 = 0 \tag{33}$$

Since (33) represents a second-order linear dynamic system, a simple method that ensures the stability of (32) is selecting β_1 and β_2 as

$$\beta_1 = 2\omega_0, \beta_2 = \omega_0^2 \tag{34}$$

where ω_0 is the bandwidth of the LESO. Then, the estimation error of the *LESO* in steady-state is

$$\begin{aligned}\tilde{x}_{1i,s} &= \lim_{p\to 0} \frac{f_i}{p^2 + \beta_1 p + \beta_2} = \frac{f_i}{\omega_0^2} \\ \tilde{x}_{2i,s} &= \lim_{p\to 0} \frac{\beta_1 f_i + \dot{f}_i}{p^2 + \beta_1 p + \beta_2} = \frac{2\omega_0 f_i + \dot{f}_i}{\omega_0^2}\end{aligned} \tag{35}$$

Second, by taking (27) and (35) into consideration, it can be concluded that the *LESO*'s estimation error is bounded by

$$\begin{aligned}|\tilde{x}_{1i,s}| &\le \frac{\varepsilon_1}{\omega_0^2} \\ |\tilde{x}_{2i,s}| &\le \frac{2\omega_0\varepsilon_1 + \varepsilon_2}{\omega_0^2}\end{aligned} \tag{36}$$

3.3. Model-free Sliding Mode Control Design

As seen in (24), the *iPD* controller can perform well as the LESO is perfect. However, sensitivity to measurement noise as well as high sampling rate requirement which needs more powerful hardware are two major issues when a large bandwidth ω_0 is chosen in practice. Nevertheless, if a lower bandwidth is selected, the *LESO* estimation error increases as pointed out in (36), and following that the performance of the simple *iPD*-based model-free control is degraded. Hence, an additional SMC is proposed to suppress the influence of this remaining estimation error. The control design of the SMC is presented in this section, in detail.

The traditional SMC law u_{smc} is comprised of two fundamental components: an equivalent control signal and another switching term. The equivalent control action u_{eq} is responsible for driving the system's states towards the sliding surface, which is a hyperplane that separates the desired and undesired states of the system. On the other hand, the switching control term u_{sw} ensures that the system's states remain on the sliding surface, which is essential for achieving stability and robustness in the control system. However, the problem of chattering is an inherent limitation that hinders the widespread adoption of the SMC. In this section, a model-free SMC using the double power reaching law in combination with ULM is designed. This approach not only guarantees that the sliding surface is quickly reached but also effectively reduces the chattering phenomenon. Now, consider the following SMC signal

$$u_{smc} = u_{eq} + u_{sw} \tag{37}$$

By augmenting the existing iPD controller (21) with an additional control signal u_{smc}, it yields

$$\boldsymbol{u} = \frac{1}{\alpha}(K_p\boldsymbol{e} + K_D\dot{\boldsymbol{e}} + \ddot{\boldsymbol{q}}_{\boldsymbol{ref}} - \hat{\boldsymbol{F}}) + \boldsymbol{u}_{\boldsymbol{smc}} \tag{38}$$

Substitute (38) into (19), then the dynamic of the tracking error is

$$\ddot{\boldsymbol{e}} + \alpha\boldsymbol{u}_{\boldsymbol{smc}} + K_p\boldsymbol{e} + K_D\dot{\boldsymbol{e}} = \tilde{\boldsymbol{F}} \tag{39}$$

Chose the sliding surface $\boldsymbol{s}$ as follows:

$$\boldsymbol{s} = \dot{\boldsymbol{e}} + \lambda\boldsymbol{e} \tag{40}$$

In which, λ is a positive constant. Then, by taking the derivative on both sides of (40), it gives

$$\dot{\boldsymbol{s}} = \ddot{\boldsymbol{e}} + \lambda.\dot{\boldsymbol{e}} \tag{41}$$

Now, by extracting $\ddot{\boldsymbol{e}}$ from (39) and substituting it into (41), the dynamic of the sliding surface can be represented by

$$\dot{\boldsymbol{s}} = \tilde{\boldsymbol{F}} - (\alpha\boldsymbol{u}_{\boldsymbol{smc}} + K_p\boldsymbol{e} + K_D\dot{\boldsymbol{e}}) + \lambda\dot{\boldsymbol{e}} \tag{42}$$

The equivalent control signal $\boldsymbol{u}_{eq}$ can be found by solving (42) in the case of $\dot{\boldsymbol{s}} = 0$ and neglecting the unknown term $\tilde{\boldsymbol{F}}$. As a result

$$\boldsymbol{u}_{eq} = \frac{1}{\alpha}[-K_p\boldsymbol{e} + (\lambda - K_D)\dot{\boldsymbol{e}}] \tag{43}$$

In SMC design, there are plenty of reaching laws that have been proposed in the literature to cope with the uncertainties. Among such proposed methods, the double power rate law exhibits several advantages such as faster reaching speed and less chattering. Hence, this approach is chosen in this research. Considering the following switching control signal

$$\boldsymbol{u}_{sw} = \frac{k_1}{\alpha}.|\boldsymbol{s}|^{\cdot\gamma}.sign(\boldsymbol{s}) + \frac{k_2}{\alpha}.|\boldsymbol{s}|^{\cdot\beta}.sign(\boldsymbol{s}) \tag{44}$$

with $(k_1, k_2 > 0)$, $\gamma > 1, 0 < \beta < 1$. Besides, $.|\boldsymbol{s}|^{\cdot\gamma}$, $.sign(\boldsymbol{s})$ mean element-wise operation. Substitute (43), (44) into (42) with consideration of (37), it gives

$$\dot{\boldsymbol{s}} = \tilde{\boldsymbol{F}} - k_1.|\boldsymbol{s}|^{\cdot\gamma}.sign(\boldsymbol{s}) - k_2.|\boldsymbol{s}|^{\cdot\beta}.sign(\boldsymbol{s}) \tag{45}$$

In (45), the two terms $k_1.|\boldsymbol{s}|^{\cdot\gamma}.sign(\boldsymbol{s})$ and $k_2.|\boldsymbol{s}|^{\cdot\beta}.sign(\boldsymbol{s})$ respectively play a dominant role as $|\boldsymbol{s}| > 1$ and $|\boldsymbol{s}| < 1$, while the influence of the remaining part is weakened. Due to this characteristic, this law guarantees a consistently fast-reaching speed for the control system. Finally, by taking summation of (43) and (44), the final employed SMC law is

$$\boldsymbol{u}_{smc} = \frac{1}{\alpha}[-K_p\boldsymbol{e} + (\lambda - K_D)\dot{\boldsymbol{e}} + k_1.|\boldsymbol{s}|^{\cdot\gamma}.sign(\boldsymbol{s}) + k_2.|\boldsymbol{s}|^{\cdot\beta}.sign(\boldsymbol{s})] \tag{46}$$

And the final control signal is obtained by substituting (46) into (38), which results in

$$\boldsymbol{u} = \frac{1}{\alpha}[\ddot{\boldsymbol{q}}_{ref} + \lambda\dot{\boldsymbol{e}} + k_1.|\boldsymbol{s}|^{\cdot\gamma}.sign(\boldsymbol{s}) + k_2.|\boldsymbol{s}|^{\cdot\beta}.sign(\boldsymbol{s}) - \hat{\boldsymbol{F}}] \tag{47}$$

4. Stability analysis

First, the stability of the *LESO* is guaranteed by (34). Then, the stability of the control system is actually dependent on (45). Considering the following candidate Lyapunov function:

$$\boldsymbol{V} = \frac{1}{2}\boldsymbol{s}^T\boldsymbol{s} \tag{48}$$

Differentiate both sides of (48) and take (45) into account, it yields

$$\begin{aligned} \dot{\boldsymbol{V}} &= \boldsymbol{s}^T \dot{\boldsymbol{s}} \\ &= \boldsymbol{s}^T (\tilde{\boldsymbol{F}} - k_1.|\boldsymbol{s}|^{\cdot\gamma}.sign(\boldsymbol{s}) - k_2.|\boldsymbol{s}|^{\cdot\beta}.sign(\boldsymbol{s})) \end{aligned} \tag{49}$$

Equation (49) can be rewritten in detail as

$$\dot{V}_i = s_i[\tilde{f}_i - k_1|s_i|^{\gamma}sign(s_i) - k_2|s_i|^{\beta}sign(s)]; \quad \boldsymbol{with} \quad i = (1,2,3) \tag{50}$$

As previously discussed, the reaching phase of the double power reaching law can be divided into two regions, corresponding to $|s_i| > 1$ and $|s_i| \leq 1$. In the former region, $k_1|s_i|^{\gamma}sign(s_i)$ is dominant while $k_2|s_i|^{\beta}sign(s)$ is essential in the latter one. Therefore, the stability analysis can also be performed in those two regions respectively.

First, suppose that $s_i > 1$, then (50) can approximately represented by

$$\dot{V}_i \approx s_i[\tilde{f}_i - k_1 s_i^{\gamma}] \tag{51}$$

As referred from (36), $|\tilde{f}_i| = |\tilde{x}_{2i,s}| \leq \frac{2\omega_0\varepsilon_1 + \varepsilon_2}{\omega_0^2}$. Then (51) fulfills

$$\begin{aligned} \dot{V}_i &\approx s_i[\tilde{f}_i - k_1 s_i^{\gamma}] \\ &< s_i[\frac{2\omega_0\varepsilon_1 + \varepsilon_2}{\omega_0^2} - k_1 s_i^{\gamma}] \end{aligned} \tag{52}$$

Inequality (52) shows that the stability of the control system in this phase can be guaranteed by choosing k_1 so that $\dot{V}_i < 0$ for all $s_i > 1$ and $\gamma > 1$. Therefore,

$$\begin{aligned} k_1 &> \max[\frac{1}{s_i^{\gamma}}(\frac{2\omega_0\varepsilon_1 + \varepsilon_2}{\omega_0^2})] \\ \rightarrow k_1 &> \frac{2\omega_0\varepsilon_1 + \varepsilon_2}{\omega_0^2} \end{aligned} \tag{53}$$

Similarly, consider the situation where $0 < s_{i,min} < s_i < 1$, in which $0 < s_{i,min} << 1$ is a small expected boundary. Then (50) can be reformulated by

$$\dot{V}_i \approx s_i[\tilde{f}_i - k_2 s_i^{\beta}] \tag{54}$$

To guarantee the stability of the control system in this case, k_2 must be selected such that $\dot{V}_i < 0$. Consequently,

$$\begin{aligned} &k_2 > \max \frac{\tilde{f}_i}{s_i^{\beta}} \\ \rightarrow &k_2 > [\frac{1}{s_{i,min}^{\beta}}(\frac{2\omega_0\varepsilon_1 + \varepsilon_2}{\omega_0^2})] \end{aligned} \tag{55}$$

By chosing k_1 and k_2 according to (52) and (55), $\dot{V}_i < 0$ is also true in the case where $s_i < -1$ and $-1 < s_i < -s_{i,min} < 0$, respectively. This means the sliding variable s_i approaches a small vicinity $[-s_{i,min}, s_{i,min}]$ asymptotically. As a result, the stability of the control system is guaranteed and the chattering phenomenon is restricted in a small region $[-s_{i,min}, s_{i,min}]$.

5. Numerical simulations and discussions

Table 3. System's Parameters

Symbol	Description	Symbol	Description
a	0.3(m)	b	0.3(m)
m	40(kg)	R	0.075(m)
I	6(N·m)	f_i	10(N)
D_θ	0.2	λ	3
k_1	0.8	k_2	0.8
α	1.2	β	0.6
ω_0	100(rad/s)		

In this section, various numerical simulations are carried out to determine the effectiveness of the proposed trajectory-tracking control system. The parameters of the 4-MWMR and the controller are provided in Table 3. Two typical references including step and circular trajectories are employed in simulations. In addition, the proposed controller is also compared with the iPD controller and the classical SMC to show a more comprehensive evaluation.

Define the reference trajectory $\boldsymbol{q_{ref}}$ as

$$\boldsymbol{q}_{ref} = \begin{bmatrix} x_{ref}(t) \\ y_{ref}(t) \\ \phi_{ref}(t) \end{bmatrix} \tag{56}$$

Then, a step change trajectory can be described by

$$x_{ref} = \begin{cases} 0, t < 10 \\ 0.1(t-10), t \geq 10 \end{cases}$$
$$y_{ref} = \begin{cases} 0.1t, t < 10 \\ 1, t \geq 10 \end{cases} \tag{57}$$
$$\phi_{ref} = \begin{cases} 0, t < 10 \\ 0, t \geq 10 \end{cases}$$

This means the 4-MWMR moves along the y axis in the first 10 seconds and turns right suddenly after that without rotating its body.

The employed circular trajectory is represented by

$$\boldsymbol{q}_{ref} = \begin{bmatrix} x_{ref}(t) \\ y_{ref}(t) \\ \phi_{ref}(t) \end{bmatrix} = \begin{bmatrix} 0.6sin(0.2t)(m) \\ 0.6cos(0.2t)(m) \\ 0.6sin(0.2t)(rad) \end{bmatrix} \tag{58}$$

In the first scenario, simulations are conducted under ideal conditions where all parameters are constant and no modeling errors, as well as disturbances, exist. Simulation results with step and circular reference trajectories are shown in Fig. 3 and Fig 4, respectively.

By observing the above-mentioned results, it can be seen that all three controllers including iPD, SMC, and iPDSMC can drive the 4-MWMR to track the reference trajectories

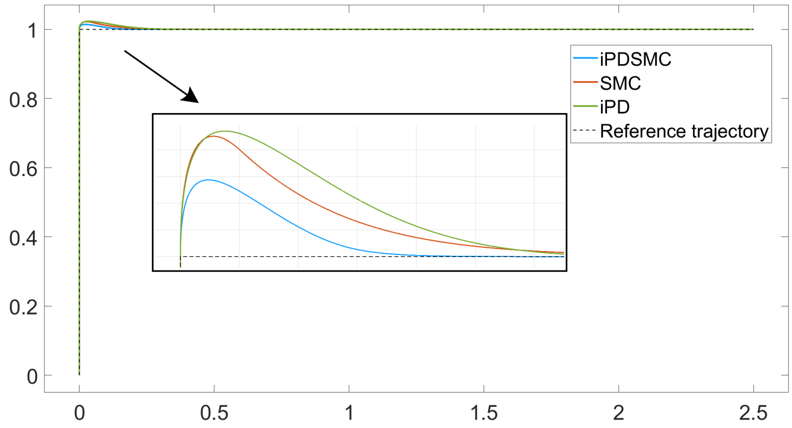

Fig. 3. Tracking performance under ideal conditions with step trajectory

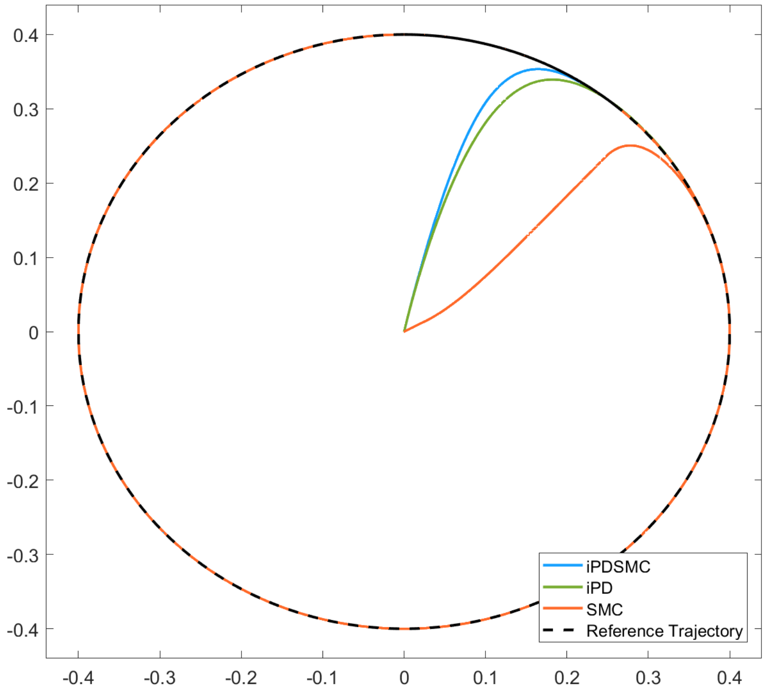

Fig. 4. Tracking trajectory under ideal condition with circular trajectory

asymptotically. In addition, none of the three controllers exhibit steady-state errors.

In the second scenario, simulations are conducted under the influence of the following lumped disturbance

$$\tau_d = \begin{bmatrix} 0.5sin(2t) & 0.5cos(2t) & 0.5sin(2t) & 0.5 * cos(2t) \end{bmatrix}^T \tag{59}$$

Simulation results shown in Fig. 5 and Fig. 6 indicate that under the affection of the unmatched disturbance (36), the classical SMC is no longer able to control the 4-MWMR to

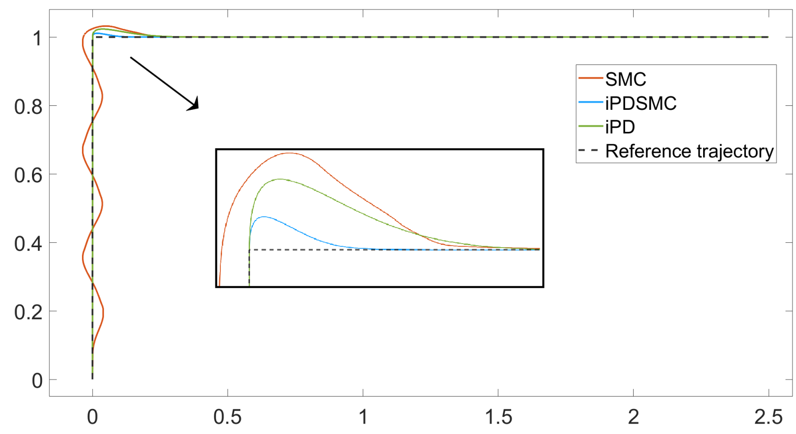

Fig. 5. Tracking performance with step trajectory under disturbance

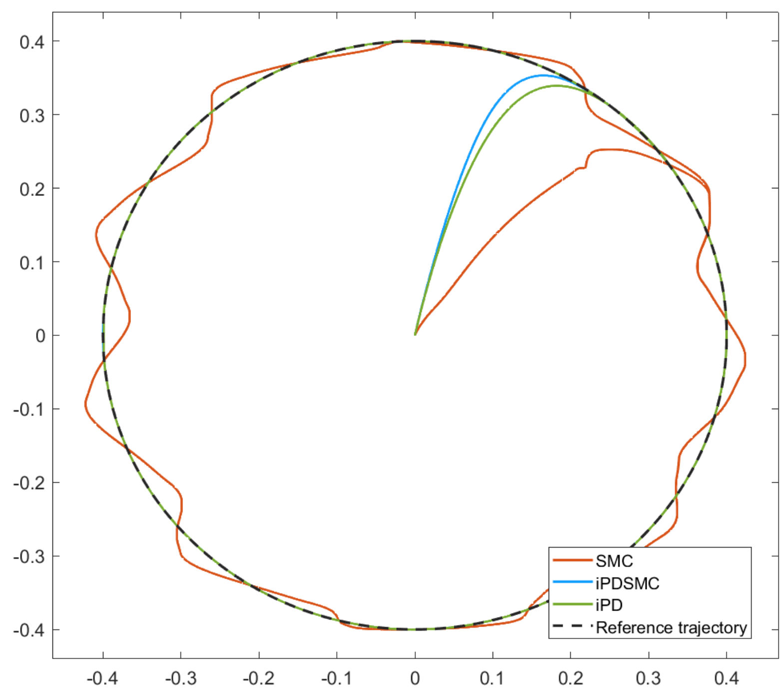

Fig. 6. Tracking performance with circle trajectory under disturbance

track the reference trajectory in both cases. In contrast, both iPDSMC and iPD controllers still perform well without steady-state error. Both above simulation results show that there is no remarkable difference between the iPD and the $iPDSMC$-based model-free control in terms of tracking performance. The main reason is that the bandwidth ω_0 of the $LESO$ is sufficiently large, i.e., $100(rad/s)$, so that the estimation error of the $LESO$ can be neglected.

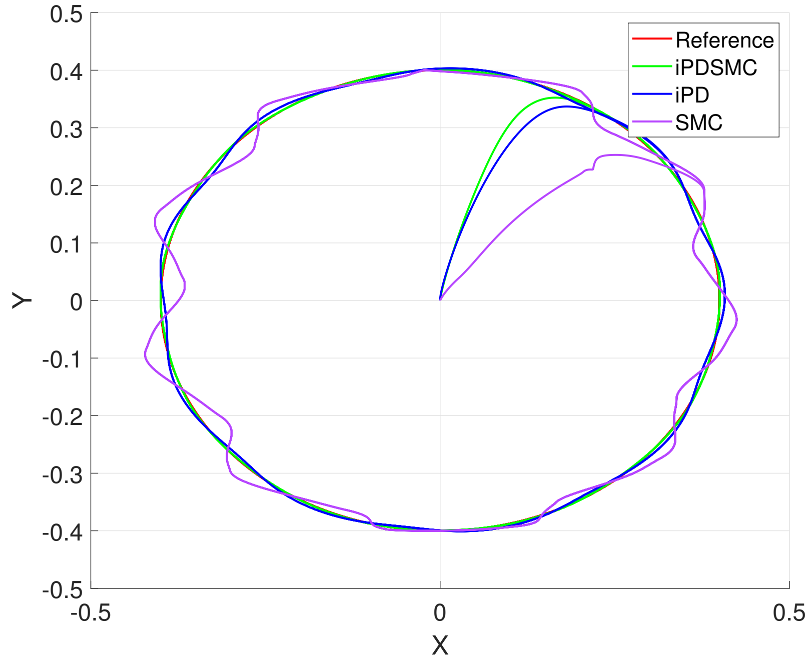

Fig. 7. Circular trajectory tracking control with $\omega_0 = 50(rad/s)$

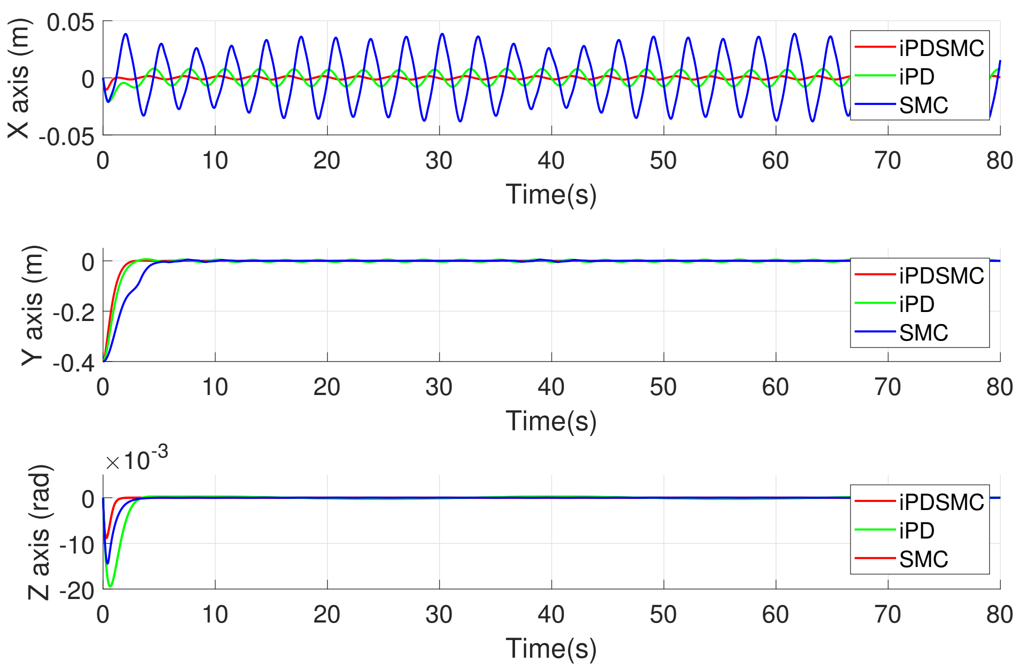

Fig. 8. Tracking error with with $\omega_0 = 50(rad/s)$

To show the advantage of the proposed $iPDSMC$ over the classical $iPDSMC$, simulations with a lower bandwidth, i.e., $\omega_0 = 50(rad/s)$ are conducted, and the results are shown in Fig. 7 and Fig. 8. It can easily be seen that the tracking performance of the iPD controller degrades significantly as ω_0 decreases. In contrast, the proposed $iPDSMC$ maintains its performance with unnoticeable changes.

6. CONCLUSIONS

In this research, the trajectory tracking control problem of a 4-MWMR based on the model-free control strategy is presented. This approach eliminates the time-consuming effort that is used to build a precise mathematical model for control design. Theoretical analysis is carried out, which shows that the performance of the control system not only depends on the parameters of the classical iPD controller but also the bandwidth of the LESO which continuously updates the unknown lump disturbances. Then, an $iPDSMC$ control strategy is proposed to guarantee the balance between measurement noise immunity, hardware cost, and control system performance. Numerical simulations show that at low LESO bandwidth, the proposed strategy performs much better than the classical iPD controller in terms of tracking accuracy. This contribution is meaningful in practice since a low LESO bandwidth gives the control system the ability to reject the high-frequency noise influences. Besides, the cheaper controllers can be used due to the fact that the sampling rate of the control system can be diminished along with the bandwidth.

Conflicts of Interest: The author declares no conflict of interest.

Acknowledgment

This research is funded by the Hanoi University of Science and Technology (HUST) under project number T2022-PC-005.

References

[1] K. Jayabalan, Sangeetha, B. Tanneru, H. Prasad, and V. Mukkoti, (2017) *"A Mecanum Wheel Based Robot Platform for Warehouse Automation"* **International Journal of Mechanical Engineering and Technology** *8*: 181–189.

[2] Y. Shi, A. Hayat, V. Sivanantham, and R. E. Mohan, (2021) *"WaspL: Design of a Reconfigurable Logistic Robot for Hospital Settings"*:

[3] B. Clemons, I. Ferdyan, and K. Anderson, (2022) *"The Development of E-Butler Hotel Service Robot"* **Engineering, MAthematics and Computer Science (EMACS) Journal** *4*: 67–72. DOI: 10.21512/emacsjournal.v4i2.8119.

[4] R. Galati, G. Mantriota, and G. Reina, (2022) *"Adaptive heading correction for an industrial heavy-duty omnidirectional robot"* **Scientific Reports** *12*: DOI: 10.1038/s41598-022-24270-x.

[5] A. Ma'arif, N. Raharja, G. Supangkat, F. Arofiati, R. Sekhar, and D. Rijalusalam, (2021) *"PID-based with Odometry for Trajectory Tracking Control on Four-wheel Omnidirectional Covid-19 Aromatherapy Robot"* **Emerging Science Journal** *5*: 157–181. DOI: 10.28991/esj-2021-SPER-13.

[6] N. Hong Thai, T. Ly, and L. Dzung, (2022) *"Trajectory tracking control for mecanum wheel mobile robot by time-varying parameter PID controller"* **Bulletin of Electrical Engineering and Informatics** *11*: 1902–1910. DOI: 10.11591/eei.v11i4.3712.

[7] P. Wu, K. Wang, J. Zhang, and Q. Zhang, (2017) *"Optimal Design for PID Controller Based on DE Algorithm in Omnidirectional Mobile Robot"* **MATEC Web of Conferences** *95*: 08014. DOI: 10.1051/matecconf/20179508014.

[8] S. Morales, J. Magallanes, C. Delgado, and R. Canahuire. "LQR Trajectory Tracking Control of an Omnidirectional Wheeled Mobile Robot". In: 2018, 1–5. DOI: 10.1109/CCRA.2018.8588146.

[9] T. Zhang and X. Zhang, (2023) *"Distributed Model Predictive Control with Particle Swarm Optimizer for Collision-Free Trajectory Tracking of MWMR Formation"* **Actuators *12***: 127. DOI: 10.3390/act12030127.

[10] C. Wang, X. Liu, X. Yang, F. Hu, A. Jiang, and C. Yang, (2018) *"Trajectory Tracking of an Omni-Directional Wheeled Mobile Robot Using a Model Predictive Control Strategy"* **Applied Sciences *8***: 231. DOI: 10.3390/app8020231.

[11] D. Wang, W. Wei, Y. Yeboah, Y. Li, and Y. Gao, (2020) *"A Robust Model Predictive Control Strategy for Trajectory Tracking of Omni-directional Mobile Robots"* **Journal of Intelligent Robotic Systems *98***: DOI: 10.1007/s10846-019-01083-1.

[12] I. Moreno, E. Celaya, and L. Ros, (2021) *"Model Predictive Control for a Mecanum-wheeled Robot Navigating among Obstacles"* **IFAC-PapersOnLine *54***: 119–125. DOI: 10.1016/j.ifacol.2021.08.533.

[13] Z. Islam, S. Sahoo, M. Saad, U. Tople, and A. Khandare. "Robust Backstepping Controller for an Omniwheeled Mobile Robot with Uncertainties and External Disturbances". In: 2021, 35–42. DOI: 10.1007/978-981-15-3639-7_5.

[14] L.-C. Lin and H.-Y. Shih, (2013) *"Modeling and Adaptive Control of an Omni-Mecanum-Wheeled Robot"* **Intelligent Control and Automation *04***: 166–179. DOI: 10.4236/ica.2013.42021.

[15] Z. Islam, S. Chiddarwar, and S. Sahoo. "Design of Robust Backstepping Controller for Four-Wheeled Mecanum Mobile Robot". In: 2021, 1125–1134. DOI: 10.1007/978-981-16-0550-5_107.

[16] Z. Yuan, Y. Tian, Y. Yin, S. Wang, J. Liu, and L. Wu, (2020) *"Trajectory Tracking Control of a Four Mecanum Wheeled Mobile Platform: an Extended State Observer-Based Sliding Mode Approach"* **IET Control Theory Applications *14***: DOI: 10.1049/iet-cta.2018.6127.

[17] V. Alakshendra and S. Chiddarwar, (2017) *"Adaptive robust control of Mecanum-wheeled mobile robot with uncertainties"* **Nonlinear Dynamics *87***: DOI: 10.1007/s11071-016-3179-1.

[18] Z. Sun, H. Xie, J. Zheng, Z. Man, and D. He, (2020) *"Path-Following Control of Mecanum-Wheels Omnidirectional Mobile Robots Using Nonsingular Terminal Sliding Mode"* **Mechanical Systems and Signal Processing**: DOI: 10.1016/j.ymssp.2020.107128.

[19] P. Bozek, Y. Karavaev, A. Ardentov, and K. Yefremov, (2020) *"Neural network control of a wheeled mobile robot based on optimal trajectories"* **International Journal of Advanced Robotic Systems *17***: DOI: 10.1177/1729881420916077.

[20] M. Fliess and C. Join. "Intelligent PID controllers". In: 2008, 326–331. DOI: 10.1109/MED.2008.4601995.

[21] M. Fliess and C. Join, (2013) *"Model-free control"* **International Journal of Control *86***: DOI: 10.1080/00207179.2013.810345.

[22] Y. Zhang, J. Jin, and L. Huang, (2020) *"Model-Free Predictive Current Control of PMSM Drives Based on Extended State Observer Using Ultralocal Model"* **IEEE Transactions on Industrial Electronics *PP***: 1–1. DOI: 10.1109/TIE.2020.2970660.

[23] T. Li and X. Liu, (2021) *"Model-Free Non-Cascade Integral Sliding Mode Control of Permanent Magnet Synchronous Motor Drive with a Fast Reaching Law"* **Symmetry *13***: 1680. DOI: 10.3390/sym13091680.

[24] J. Han, (2009) *"From PID to Active Disturbance Rejection Control"* **Industrial Electronics, IEEE Transactions on *56***: 900–906. DOI: 10.1109/TIE.2008.2011621.

[25] Z. Gao. "Scaling and Parameterization Based Controller Tuning". In: ***6***. 2003, 4989–4996. DOI: 10.1109/ACC.2003.1242516.

[26] C.-C. Tsai and H.-L. Wu. "Nonsingular terminal sliding control using fuzzy wavelet networks for Mecanum wheeled omni-directional vehicles". In: *International Conference on Fuzzy Systems*. 2010, 1–6. DOI: 10.1109/FUZZY.2010.5584223.